Constructing the Universe with Clusters of Galaxies, IAP 2000 meeting, Paris (France) July 2000
Florence Durret & Daniel Gerbal eds.

FIRST RESULTS ON CLUSTERS OBSERVED BY XMM-Newton/EPIC

M. ARNAUD[1], N.AGHANIM[2], E.BELSOLE[1], R. GASTAUD[3], S.MAJEROWICZ[1], D.M. NEUMANN[1], J.L. SAUVAGEOT[1]

1. CEA/DSM/DAPNIA/SAp Saclay, 91191 Gif-sur-Yvette, France
2. IAS-CNRS, Université Paris Sud, , 91405 Orsay Cedex, France
3. CEA/DSM/DAPNIA/SEI Saclay, 91191 Gif-sur-Yvette, France

We present the first XMM observations of clusters, performed during the commissioning and calibration phases. These data are used to illustrate the capabilities of XMM for poor systems study and to assess the effect of vignetting and background for the determination of temperature profiles in bright clusters.

1 Introduction

The XMM satellite (Jansen *et al.* [8]), an ESA science mission, has been launched in December 1999. The specificity of XMM lies in the exceptional collecting area of its X–ray telescopes. XMM is also unique in that it allows simultaneously non dispersive spectroscopic imaging and high resolution dispersive spectroscopy, together with a study of the UV/optical properties of the X-ray source via the coaligned Optical Monitor (OM). The EPIC instrument (Turner *et al.* [16]) on board XMM combines a high sensitivity with good spatial resolution (FWHM = 8", better than ROSAT/PSPC) and spectral resolution ($\Delta E = 60 - 140$ eV, better than ASCA), on a wide energy range (0.1 to 12 keV). The performances of the instrument are as expected, as confirmed by in-flight calibration data (Turner *et al.* [16]). The XMM/EPIC instrument is specially well suited for the study of cluster of galaxies: the exceptional sensitivity, associated with good spectroscopic imaging capabilities, allows the detection and observations of clusters out to cosmological distances ($z > 1$) and very accurate determination of the gas temperature and abundances distributions in more nearby ones.

In this paper we illustrate some capabilities of XMM/EPIC for cluster study, using the three observations of clusters done in the commissioning and calibration phase. More scientific results can be found in the special issue on XMM, where PV observations of Virgo/M87 (Böhringer *et al.* [6]; Belsole *et al.* [3]), Coma (Arnaud *et al.* [1]; Briel *et al.* [7]; Neumann *et al.* [10]), A1795 (Arnaud *et al.* [2]; Mittaz *et al.* [9]; Tamura *et al.* [14]) and A1835 (Peterson *et al.* [12]) are discussed.

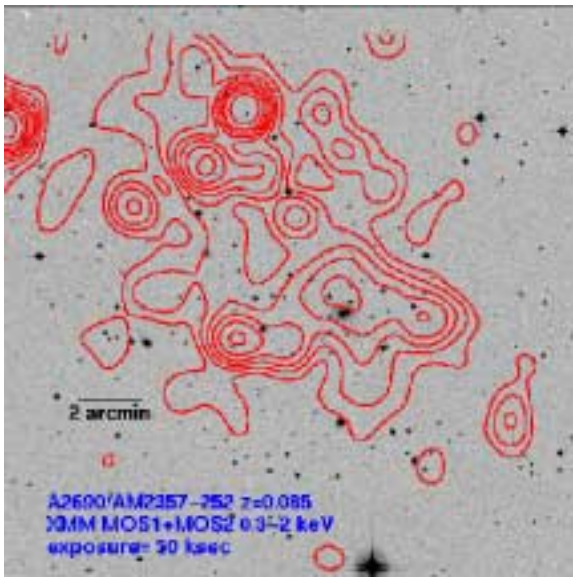

Figure 1: X-ray image of A2690 in the 0.3-2 kev energy band from XMM/EPIC/MOS data (30 ksec exposure) overlayed on the DSS optical image. The lowest isocontours corresponds to 3σ detection over background. The images if filtered with a gauss filter. Point like emission is superimposed on the cluster diffuse emission.

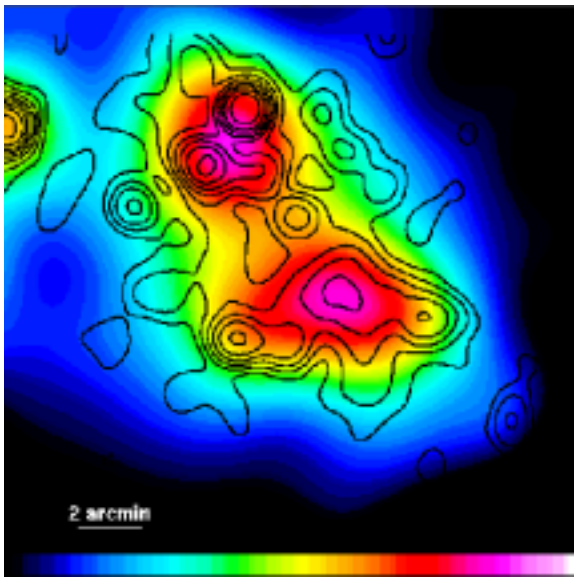

Figure 2: X-ray isocontours as in Fig. 1 overlayed on the image of the wavelet reconstructed diffuse emission. Note the bimodal structure.

2 HCG16, a compact group of galaxies

The Hickson group 16 (HCG16) was a first light target of XMM (January 2000). Poor groups of galaxies constitute the extreme poor end of the spectrum of galaxy clustering and their study is fundamental on a cosmological point of view. In particular they provide an extreme test of the various trends found in galaxy clusters. The HCG16 compact group was studied with ROSAT, but no consensus was reached on the amount of diffuse X-ray emission. Precise X-ray observations are important because i) they can establish unambiguously the reality of such poor groups: the detection of diffuse X-ray emission from a hot intergalactic gaseous component gives evidence of a true gravitational potential well and thus that the overdensity in galaxies is not due to a chance projection effect ii) a precise determination of the gas content and temperature of such poor systems allows to check the importance of non-gravitational effects, like gas loss and heating due to galaxy feedback.

The XMM observation of HCG16 demonstrates the capability of XMM to address these issues. Thanks to XMM sensitivity and good spatial resolution, diffuse emission has been unambiguously detected (thus confirming the reality of this group) and separated from point like emission and a precise determination of temperature and luminosity derived. We refer the reader to the paper by Belsole *et al.*[4] for a detailed presentation of the imagery and spectroscopic analysis and the scientific discussion on this object.

3 A2690, a poor unrelaxed cluster

In the standard hierarchical models of structure formation, the build-up of structures occurs through continuous mergers of smaller previously collapsed structures. This formation process is going on now at cluster scale. Dynamic studies of these objects (in particular of merger events), over a wide range of cluster masses, are needed to constrain cosmological scenario of

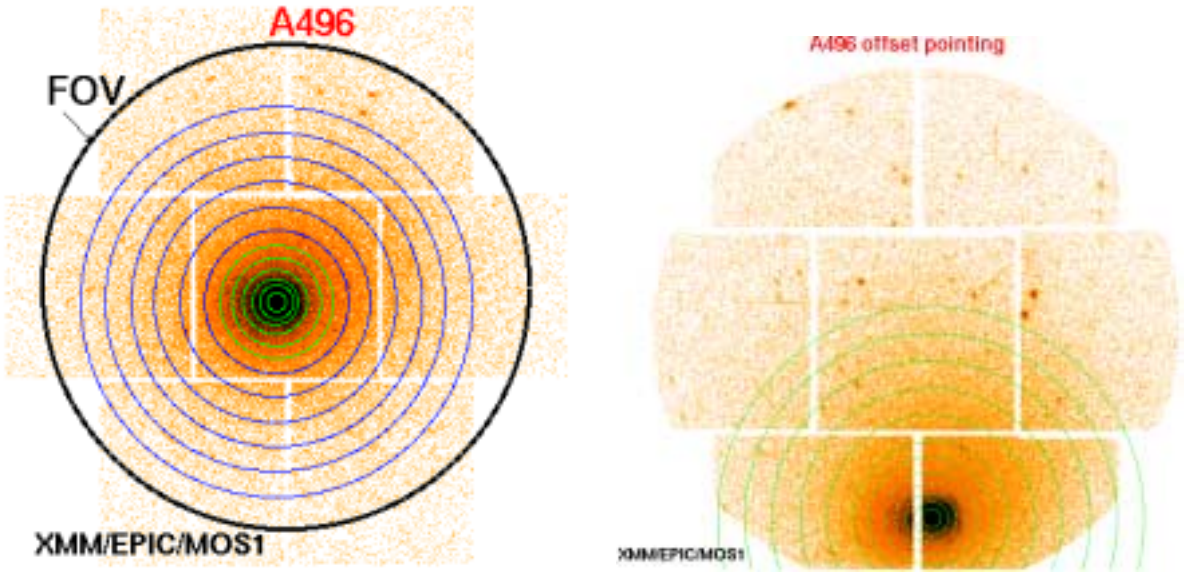

Figure 3: XMM/EPIC/MOS1 image of A 496 in the [0.2 – 10] keV energy band (logarithmic intensity) for the on-axis pointing (left panel) and off-axis pointing (right panel). The green circles define the extraction regions used in the spectroscopic analysis. The black circle in the left panel delineates the instrument FOV. Outside this circle the detector is masked by the proton shield. Note the residual emission, which is due to the CR induced background.

structure formation and understand how cluster form and evolve.

A2690 is a cluster at z=0.085, observed by XMM as a calibration target for the Optical Monitor. No previous X-ray data existed for this cluster. An EPIC/MOS image is shown on Fig. 1 overlayed on the optical image from the DSS. The cluster appears irregular. The diffuse emission was reconstructed using a Wavelet-based technics (Bijaoui & Rué[5], and Rué & Bijaoui[13]), revealing a bimodal structure. This suggests that the cluster is presently undergoing a merger event. We also extracted the spectrum of the diffuse emission and derived a temperature of $kT = 1.3 \pm 0.5$ keV and a bolometric luminosity of 3 10^{43} ergs/s. Note that these values are consistent with the luminosity-temperature relation derived by Arnaud & Evrard (2000). This preliminary analysis clearly shows that the dynamic state of even very poor clusters can be studied with XMM up to $z \sim 0.1$.

4 Spectro-imagery of bright clusters: the effect of vignetting and background

The determination of the temperature profiles of the hot gas in galaxy clusters is essential to derive the gas entropy distribution and to measure the total mass content, through the equation of hydrostatic equilibrium. Significant progress in this field was expected with XMM-Newton/EPIC, which has a much better sensitivity than ASCA and SAX and does not suffer from the large energy dependent PSF of ASCA, a major source of systematic uncertainty. A proper treatment of the background and vignetting effects are nonetheless required when analyzing extended sources like cluster of galaxies. We first studied these effects using XMM observations of the A496 cluster. This calibration target is part of the guaranteed time program and the results presented here are by courtesy of Dr J.Bleeker. A496 is a bright cluster, which was observed on axis and off axis, allowing to check the vignetting correction (Fig.3). We refer the reader to the paper by Tamura *et al.*[15] for scientific results on this cluster.

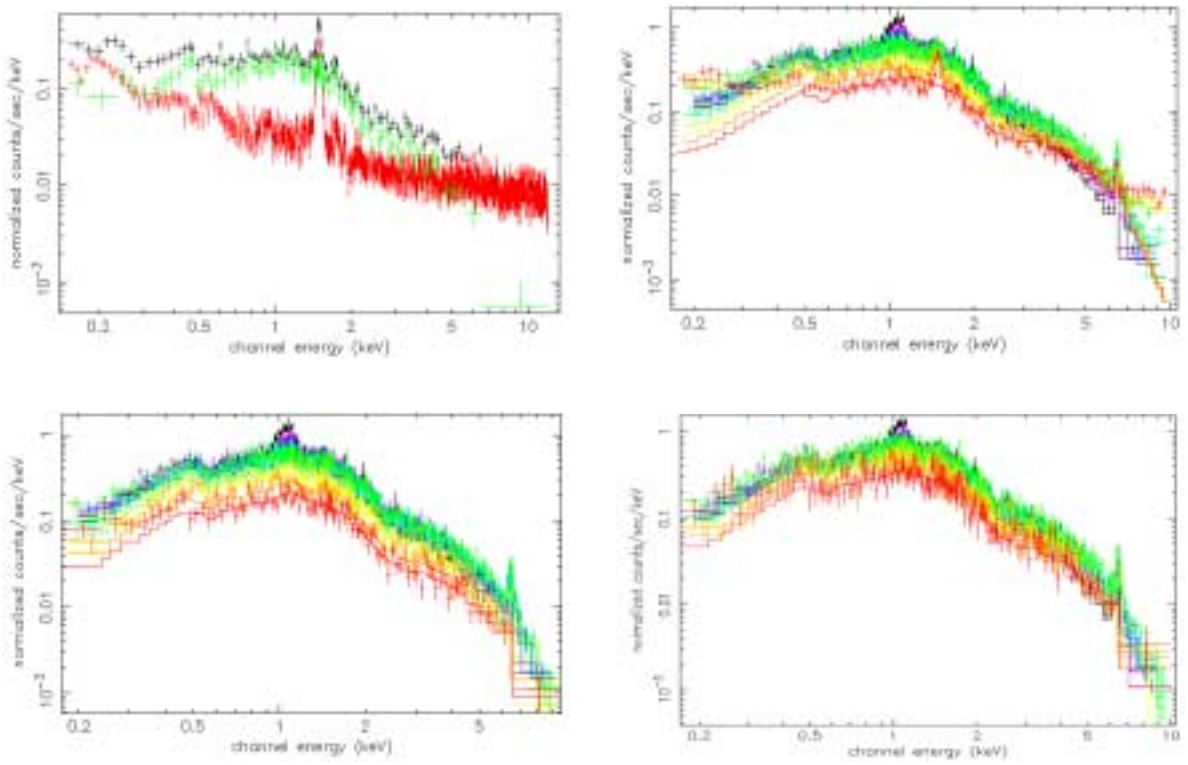

Figure 4: XMM/EPIC/MOS1 spectra of A496 from the on-axis observation. **Top left panel**: Spectra in the $8.7' - 10.2'$ region. Black points: raw spectrum. Red points: the background spectrum derived from the LH observation. Green points: the corresponding background subtracted cluster spectrum. **Top right left panel:** Raw spectra in the concentric rings defined in Fig. 3. The spectra from inner to outer regions are colored following the rainbow color order (purple is for the inner ring and red for the outer ring). Note the high energy tails, more and more prominent with distance to the cluster center. The continuous lines correspond to the best fit isothermal models. **Bottom left panel:** Corresponding background subtracted spectra. **Bottom right panel:** The spectra are corrected for vignetting effect and background subtracted.

4.1 Background effect

After exclusion of periods of high background induced by solar flare protons, the remaining observing time is 16 ksec and 35 ksec for the on-axis and off-axis observations respectively. Spectra in concentric rings centered on the cluster peak were extracted from the MOS1 event files (Fig. 3). The background in the quiescent periods is dominated by the cosmic X–ray background at low energy and the Cosmic Ray (CR) induced background at energies above typically 1.5 keV. To estimate the background we used the Lockman Hole (LH) observations and consider the same extraction regions (in detector coordinates) for the background than for the source, the CR induced background changing slightly in the FOV. Figure 4 (Top left panel) shows the raw cluster spectrum in the $8.7' - 10.2'$ region, the background spectrum derived from the LH observation and the corresponding background subtracted spectrum. Note the Al and Si fluorescence lines in the background spectrum and the very hard continuum above 2 keV typical of CR induced background. As a result, even for a bright cluster like A496, the background dominates the emission at high energies, even relatively close to the cluster center (here for radii greater than $\sim 5'$). The increasing importance of the CR induced background can be seen on Fig. 4 (top right panel), which shows the raw spectra in the various rings: a high energy tail is more and more prominent as one is moving away from the cluster center. If this background is not subtracted the effect on the derived temperature profile is dramatic: the fit is poor (Fig.4, top right panel) and the derived temperature are overestimated above $\theta > 4'$, the error strongly

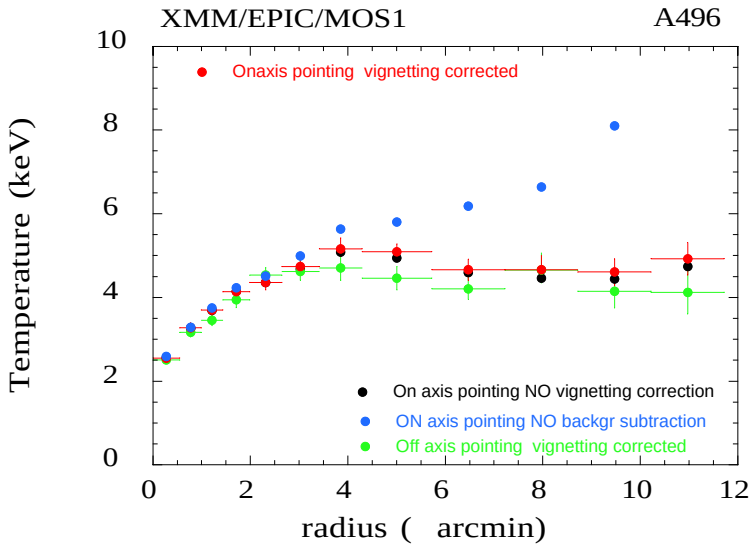

Figure 5: Radial temperature profile as a function of angular radius derived from the on-axis observation (spectra presented in Fig.4) and from the off-axis observation. An isothermal model has been fitted to the various spectra. When no background subtraction is performed the temperature is strongly overestimated (blue points, to be compared with the black points). When the spectra are corrected for vignetting effect (red points), the derived temperature is slightly higher than when this effect is not taken into account (black points). The correction is more important in the outer regions as expected, but the effect is small. The green points are derived from the background subtracted vignetting corrected spectra from the off-axis pointing. Although the on-axis and off-axis profiles are consistent, some systematic discrepancy remains of the order of the statistical errors.
WARNING: The cluster profile presented here must not be used for quantitative scientific analysis: the on-axis response matrix used in the fits was an early version, which proved to underestimate the response at low energy.

increasing with radius (Fig. 5). Further details on the background subtraction method can be found in Arnaud *et al.*[2].

4.2 Vignetting effect

While the XMM-Newton/MOS spectral resolution does not show spatial variations, the effective area at a given energy does depend on position. This vignetting effect (decrease of effective area with off-axis angle) increases with energy. This effect has to be taken into account to avoid bais in the determination of the temperature profile: If not taken into account it yields to an underestimate of the temperature increasing with off-axis angle.

We designed a simple unbiased method to correct for vignetting effects. When extracting the spectrum of a region, we weight each photon falling at position (x_j, y_j) of the detector and of energy E_j by the ratio of the effective area at that position, to the central effective area (for this energy). This weighting is taken into account in the error estimate. The 'corrected' spectrum obtained is an estimate of the spectrum one would get if the detector was flat. The spectra are fitted with XSPEC using a MEKAL model. Since the spectra are 'corrected' for vignetting effects, we can use the on axis MOS response file when fitting every spectrum. A more detailed description of the method and of the vignetting calibration data used are given in Arnaud *et al.*[2].

The vignetting corrected spectra can be compared to the non corrected spectra in Fig.4 (bottom panels). The overall normalization of the spectra is higher after vignetting correction, the increase being more important for outer rings. There is also a slight change in the spectral shape, which can be specially noticed in the outer rings: the corrected spectrum is harder. The effect is small however, the energy dependence of the vignetting correction essentially starts above an energy of 5 keV (see Neumann[11]). The vignetting correction is thus expected to be

more and more important as the cluster temperature increases. This explains why the effect on the derived temperature profile is small (compare red and black points in Fig.5) for A496: this cluster is not very hot (k$T \sim 5$ keV).

The validity of the vignetting correction can be assessed by comparing the fitted temperature of the same ring in the on-axis and off-axis pointings. The corresponding profiles (Fig. 5 red and green points). The profiles are consistent within the errors bars, but some systematic remains. Part of it could be due to intrinsic azimuthal variations in the temperature profile, the off-axis pointing covering only about half of the considered rings.

4.3 Conclusion

Both vignetting effects and background subtraction are reasonably well understood for cluster temperature profile determination. The improvement in accuracy and spatial resolution of the profile as compared to previous missions must be noticed.

5 The A1795 cluster

Preliminary results were presented at the conference. Several papers on this cluster are now in press (for the A&A special issue on XMM) and we refer the reader to these articles quoted in the introduction (Arnaud *et al.*[2]; Tamura *et al.*[14]; Mittaz *et al.*[9]). Note that no soft excess is observed above 0.3 keV in the spectrum (Fig. 4 of Arnaud *et al.*[2]), below this energy a possible excess could not be studied at the time of the paper writing, due to remaining calibration uncertainties.

Acknowledgments

We thank Dr. J. Bleeker and Dr Kaastra for making available the A496 data for calibration purpose. The work presented here is based on observations obtained with XMM-Newton, an ESA science mission with instruments and contributions directly funded by ESA Member States and the USA (NASA). EPIC was developed by the EPIC Consortium led by the Principal Investigator, Dr. M. J. L. Turner. The consortium comprises the following Institutes: University of Leicester, University of Birmingham, (UK); CEA/Saclay, IAS Orsay, CESR Toulouse, (France); IAAP Tuebingen, MPE Garching,(Germany); IFC Milan, ITESRE Bologna, IAUP Palermo, Italy. EPIC is funded by: PPARC, CEA, CNES, DLR and ASI.

References

1. Arnaud, M., Aghanim, A., Gastaud, R., Neumann , D.M., Lumb, D., Briel, U.G., Altieri, B., Ghizzardi, S., Mittaz, J.P.D., Sasseen T.P., Vestrand, W.T. *A&A* **special XMM issue**, (2001), astro-ph/0011086
2. M. Arnaud, D.M. Neumann, N. Aghanim, R. Gastaud, S.Majerowicz, J.P.Hughes, *A&A* **special XMM issue**, (2001), astro-ph/0011198
3. E. Belsole, Sauvageot J.L., Bohringer, H., Worral, D.M., Matsushita, K., Mushotzky, R.F., Sakelliou, I., Molendi, S., Ehle, M., Kennea, J., Stewart, G., Vestrand, W.T.,*A&A* **special XMM issue**, (2001), astro-ph/0011357
4. E. Belsole, E.,J.L. Sauvageot, T.Ponamn, M.Arnaud, these proceedings.
5. A. Bijaoui, F. Rué F., *Signal Processing 46* **3**, 345 (1995)
6. H.Böhringer, E.Belsole, J. Kennea, K. Matsushita, S.Molendi, D.Worrall, R.Mushotzky, M. Ehle, M.Guainazzi,I.Sakelliou, G. Stewart, W. T.Vestrand, S. Dos Santos, *A&A* **special XMM issue**, (2001), astro-ph/0011357

7. Briel, U., Henry, J.P., Lumb, D.H., Arnaud, M., Neumann, D.M., Aghanim, N., Gastaud, R., Mittaz, J.P.D., Sasseen, T., Vestrand, W.T., *A&A* **special XMM issue**, (2001), astro-ph/0011323
8. F.Jansen *et al.*, *A&A* **special XMM issue**, (2001)
9. J. P. Mittaz, J. S. Kaastra, T. Tamura, A. C. Fabian, R. F. Mushotzky, J. R. Peterson, Y. Ikebe, D. H. Lumb, F. Paerels, G. Stewart, S. Truolyubov, *A&A* **special XMM issue**, (2001), astro-ph/0011119
10. D.M. Neumann, Arnaud M., Gastaud, R., Aghanim, A., Lumb, D., Briel, U.G., Vestrand, W.T., Stewart, G.T., Molendi, S., Mittaz, J.P.D., *A&A* **special XMM issue**, (2001), astro-ph/0010435
11. D.M. Neumann , 2000, Report on the in-flight vignetting calibration of the MOS cameras aboard the XMM NEWTON satellite, CEA/Saclay, France `http://xmm.vilspa.esa.es/calibration/`
12. J. R. Peterson, F. B. S. Paerels, J. S. Kaastra, M. Arnaud, T. H. Reiprich, A. C. Fabian, R. F. Mushotzky, J. G. Jernigan, I. Sakelliou, *A&A* **special XMM issue**, (2001), astro-ph/0010658
13. F. Rué F., A. Bijaoui A., *Experimental Astronomy* **7**, 129 (1997)
14. T.Tamura, J.S. Kaastra, J. R. Peterson, F. Paerels, J. P.D. Mittaz, S. P. Trudolyubov, G. Stewart, A.C. Fabian, R.F. Mushotzky, D. H. Lumb, Y. Ikebe, *A&A* **special XMM issue**, (2001), astro-ph/0010362
15. T.Tamura *et al.*, Astronomy and Astrophysics, in preparation
16. M. Turner *et al.*, *A&A* **special XMM issue**, (2001), astro-ph/0011498.